Rapid Communications

Two distinct superconducting phases and pressure-induced crossover from type-II to type-I superconductivity in the spin-orbit-coupled superconductors $BaBi_3$ and $SrBi_3$

Bosen Wang,[1,2,3,*,†] Xuan Luo,[4,†] Kento Ishigaki,[2] Kazuyuki Matsubayashi,[2] Jinguang Cheng,[1,3] Yuping Sun,[4,5,6] and Yoshiya Uwatoko[2]

[1] *Beijing National Laboratory for Condensed Matter Physics and Institute of Physics, Chinese Academy of Sciences, Beijing 100190, China*
[2] *Institute for Solid State Physics, University of Tokyo, Kashiwanoha 5-1-5, Kashiwa, Chiba 277-8581, Japan*
[3] *Songshan Lake Materials Laboratory, Dongguan, Guangdong 523808, China*
[4] *Key Laboratory of Materials Physics, Institute of Solid State Physics, Chinese Academy of Sciences, Hefei 230031, China*
[5] *High Magnetic Field Laboratory, Chinese Academy of Sciences, Hefei 230031, China*
[6] *Collaborative Innovation Center of Advanced Microstructures,Nanjing University, Nanjing 210093, China*

(Received 18 July 2018; revised manuscript received 19 September 2018; published 12 December 2018)

We report two distinct superconducting states with different crystal structures and a crossover from a type-II to a type-I superconductor (SC) in (Ba, Sr)Bi_3. The superconducting parameters are revealed to classify two SCs: $BaBi_3$ is in the weak-coupling limit on the basis of $\Delta C/\gamma_n T_c \sim 0.67$ and $2\Delta/k_B T_c \sim 3.28$ while $SrBi_3$ is a strong-coupling SC with $\Delta C/\gamma_n T_c \sim 2.41$ and $2\Delta/k_B T_c \sim 6.09$. A large Kadowaki-Woods ratio ($R_{KW} \sim 3.53a_0$) suggests an enhanced electron-electron scattering in $BaBi_3$. With increasing the pressure, the T_c of $BaBi_3$ decreases linearly at first, and then shows an abrupt increase up to 6.2 K at 0.88 GPa. This behavior can be attributed to a pressured-induced structural transition and the resulting variations of spin-orbit coupling and Fermi structures. T_c of $SrBi_3$ is suppressed monotonously by pressure. The Ginzburg-Landau parameter κ_{GL} of $BaBi_3$ decreases from 10.35 at ambient pressure (AP) to 0.86 at 1.75 GPa, and then tends to saturation. κ_{GL} of $SrBi_3$ decreases from 0.76 at AP to $1/\sqrt{2}$ at 1.20 GPa, which manifests pressured-induced crossover from a type-II to a type-I SC. Possible physical mechanisms are proposed.

DOI: 10.1103/PhysRevB.98.220506

Superconductivity is one of macroscopic quantum phenomena and has been explored for 100 years. The Ginzburg-Landau (GL) parameter $\kappa = \lambda/\xi$ (λ is the magnetic penetration depth, ξ is the coherence length) is one of the fundamental parameters. It divides superconductors (SCs) into two classes: type I ($\kappa < \frac{1}{\sqrt{2}}$) and type II ($\kappa > \frac{1}{\sqrt{2}}$) with different interface energies: ξ is smaller than λ in type-II SCs with negative interface energy and strong flux pinning. Such behavior is not possible in a type-I SC because it cannot be penetrated by the external magnetic fields [1,2]. Thus, the crossover from a type-II to a type-I SC is unusual because the magnetic fluxes can be expelled and/or made to reappear by the stimuli. As one example, $ErRh_4B_4$ undergoes a reentrant type-I superconducting state from a type-II one at ~2.4 K [3]. TaN possesses strong anisotropic superconductivity and a crossover from a type-I to a type-II SC can be induced by changing the crystal azimuth in magnetic fields [4]. Moreover, high impurities cause more pinning, and a type-I SC behaves as a type-II SC in many cases [5,6]. Theoretical calculations also indicate that the thermally induced crossover from a type-I to a type-II SC can be originated from the interaction of magnetic vortices [7]. However, the underlying mechanism is still in dispute and not universal.

Bismuth-based materials have been extensively studied due to significant spin-orbit coupling (SOC) and unconventional superconducting pairings [8,9]. $BaBi_3$ crystallizes in the tetragonal phase ($P4/mmm$) with corner-sharing Bi_6 octahedrons [10,11]. At low temperature, it enters into the superconducting state at $T_c \sim 6$ K at ambient pressure (AP). Theoretical calculations have revealed that it possesses complicated Fermi surfaces and the density of state at the Fermi level is dominated by Bi p orbitals. The enhanced SOC is pivotal to superconducting pairings by softening phonon modes and strengthening the electron-phonon coupling [10,11]. For the isoelectron substituted material $SrBi_3$, T_c reduces to ~5.6 K with cubic symmetry [12,13]. With increasing substitution in the Ba site, cubic symmetry collapses and only the $ZrSi_2$-type $CaBi_2$ stabilizes [14]. Moreover, T_c rises to 9.0 K with increasing the Na doping in the Sr site, which is attributed to the decrease of the average number of valence electrons according to Matthias rules [15]. A recent high-pressure report indicated that T_c of $BaBi_3$ increases with the pressure coefficient $dT_c/dP \sim 1.22$ K/GPa while T_c of $SrBi_3$ decreases with $dT_c/dP \sim -0.48$ K/GPa [16]. Until now, the relationship of the opposite pressure dependence and structural transition in (Ba, Sr)Bi_3 isn't clear [16], and the systematic studies on experimental divergences are still lacking. As we know, structural transition is often accompanied by different superconducting origins. For (Ba, Sr)Bi_3, the relationship of lattice instabilities and superconductivity has not been studied in depth. Combined with the enhanced SOC characteristics, pressured-induced phenomena are expected to elucidate the correlation of structural/electronic evolutions.

*Corresponding author: bswang@iphy.ac.cn
†B.W. and X.L. contributed equally to this work.

High pressure is a clean method; it shortens bond distances and manipulates band structures as well as electron correlations, which provides a distinctive tuning way to study the interplay of lattice instabilities and superconductivity. High-pressure phase diagrams are valuable in revealing the underlying mechanism. In this Rapid Communication, we report two distinct superconducting states and a crossover from a type-II to a type-I SC in spin-orbit-coupled SCs $BaBi_3$ and $SrBi_3$ under pressure. A single crystal was grown as reported [13]. Single-crystal x-ray diffraction (XRD) and powder XRD confirm they are single phase with a small Bi impurity ($<6\%$). Susceptibility was measured on a superconducting quantum interference device. Electrical transport and specific heat were collected on a commercial physical property measurement system. High-pressure susceptibility was checked in a piston-cylinder pressure cell with lead as the pressure manometers and glycerol as the pressure medium for runs 1 and 2. Lead was removed to eliminate the diamagnetic signals for run 3. Glycerol is an isotropic liquid below 2 GPa and hydrostatic pressure is retained [17].

Figure 1 shows electrical resistivity (ρ), susceptibility, and specific heat of $BaBi_3$ and $SrBi_3$. As the temperature increases, $\rho(T)$ of $BaBi_3$ shows an S-like inflection at 40 K, and then tends to saturation above 250 K. This behavior implies electron-phonon scattering comparable to the atomic lattice spacing [11]. In $SrBi_3$, $\rho(T)$ increases linearly as a function of temperature and its magnitude is three orders smaller than that of $BaBi_3$. The superconducting transition temperatures T_c^{onset} and T_c^{zero} are 6.0 and 5.95 K for $BaBi_3$, and 5.6 and 5.50 for $SrBi_3$. The transition width is less than 0.1 K. Normal-state resistivity is fitted by $\rho = \rho_0 + AT^n$, where residual resistivity $\rho_0 \sim 3.56\,\mu\Omega\,\mathrm{cm}$, $A \sim 8.54 \times 10^{-2}\,\mu\Omega\,\mathrm{cm/K^2}$, RRR $(= \rho_{300\mathrm{K}}/\rho_0) \sim 90$ for $BaBi_3$, and $\rho_0 \sim 0.11\,\mu\Omega\,\mathrm{cm}$, $A \sim 2.7 \times 10^{-4}\,\mu\Omega\,\mathrm{cm/K^3}$, RRR ~ 549 for $SrBi_3$. These features manifest high-quality crystals [11,16]. Besides, the exponent n shifts from 2 in $BaBi_3$ to 3 in $SrBi_3$, which suggests the different dominant scatterings. In Figs. 1(e) and 1(f), susceptibility is shown in zero-field-cooling (ZFC) and field-cooling (FC) processes. The shield volumes $4\pi(M/H)_{\mathrm{ZFC}}$ and $4\pi(M/H)_{\mathrm{FC}}$ are 100% and ~5% for $BaBi_3$, and ~85% and ~66% for $SrBi_3$.

In Figs. 1(g) and 1(h), specific heat $C_e(T)$ increases abruptly at T_c, as evidence of bulk SC. The analysis of $C(T) = \gamma_n T + \beta_n T^3$, where the first and second terms are the electron and the phonon contribution, gives $\gamma_n = 49.19\,\mathrm{mJ/mol\,K^2}$, $\beta_n = 13.86\,\mathrm{mJ/mol\,K^4}$ for $BaBi_3$ and $\gamma_n = 11.03\,\mathrm{mJ/mol\,K^2}$, $\beta_n = 5.84\,\mathrm{mJ/mol\,K^4}$ for $SrBi_3$, respectively. $\Delta C_e/\gamma_n T_c$ is to 0.67 for $BaBi_3$, half of 1.43 for Bardeen-Cooper-Schrieffer (BCS) weakly coupled SCs [18]; in $SrBi_3$, $\Delta C_e/\gamma_n T_c$ is 2.41, about 3.60 times larger than that of $BaBi_3$, which indicates that superconducting properties are closely related to the tetragonal-cubic structural transition. The temperature dependence of C_e/T satisfies the BCS single-gap model $C_e = C - \beta T^3 = A\exp(-\Delta/k_B T)$ and the fitting gives $2\Delta/k_B T_c \sim 3.28$ for $BaBi_3$ and 6.09 for $SrBi_3$, which suggests the different coupling strengths [3,18]. The Debye temperature Θ_D is 149 K for $BaBi_3$ and 180 K for $SrBi_3$ by $\Theta_D = 12\pi^4 NR/5\Theta_D^3$ (N is 4, and R is the gas constant). λ_{ph} is 0.98 for $BaBi_3$ and 0.93 for $SrBi_3$ by the

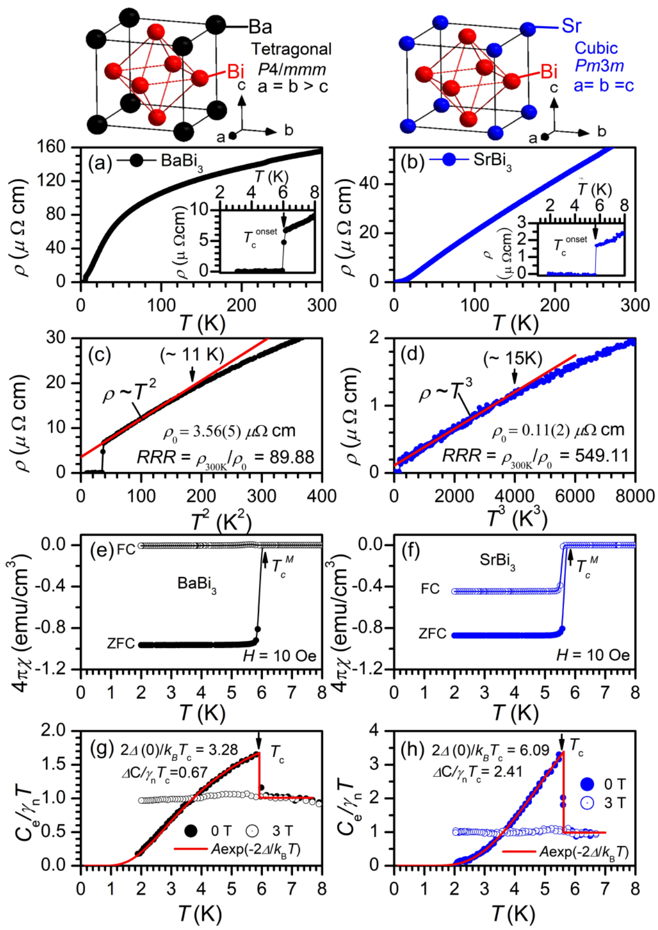

FIG. 1. Crystal structures of tetragonal and cubic phases. $\rho(T)$ of (a) $BaBi_3$ and (b) $SrBi_3$. (c) T^2 plot of resistivity and linear fitting for $BaBi_3$; (d) T^3 plot of resistivity and linear fitting for $SrBi_3$. Magnetic susceptibility of (e) $BaBi_3$ and (f) $SrBi_3$ under the ZFC/FC processes. $C_e(T)/T$ and the fittings of $C = \beta T^3 + A\exp(-\Delta/k_B T)$ where the Δ is the superconducting gap, which gives $2\Delta/k_B T_c = 3.28$ for $BaBi_3$ and 6.09 for $SrBi_3$.

McMillan formula $T_c = (\Theta_D/1.45)\exp\{-1.04(1+\lambda_{e-ph})/[\lambda_{e-ph} - \mu^*(1+0.62\lambda_{e-ph})]\}$ with $\mu^* = 0.15$ [13,18].

The electron-electron coupling constant λ_s is obtained from the enhancement of the effective mass $m^*/m_0 = \lambda_n/\gamma_n^{\mathrm{th}} = 1 + \lambda_{ph} + \lambda_s$ with $\gamma_n^{\mathrm{th}} = 2\pi^2\kappa_B^2 N(E_F)/3$ where $N(E_F)$ represents density of states at the Fermi level. In $BaBi_3$, $N(E_F) \sim 2.4$ states/eV units with SOCs [13], and $\lambda_s = m^*/m_0 - 1 - \lambda_{ph} \approx 2.33 \gg \lambda_{ph}$. Accordingly, the Kadowaki-Woods ratio $R_{\mathrm{KW}} = A/\gamma_n^2$ is $\sim 35.3\,\mu\Omega\,\mathrm{cm mol^2\,K^2/J^2}$ or $\sim 3.53\,a_0$, where $a_0 \sim 10\,\mu\Omega\,\mathrm{cm\,mol^2\,K^2/J^2}$ [19,20]. $R_{\mathrm{KW}} \sim 3.53\,a_0$ is very close to $\sim 5a_0$ in frustration materials, and 5–7 times larger than $\sim 0.5\,a_0$ in two-dimensional (2D) Fermi liquids [20,21]. The large $\lambda_s(\sim 2.33)$ and $R_{\mathrm{KW}}(\sim 3.53\,a_0)$ suggest an enhanced electron-electron scattering in $BaBi_3$. However, the m^*/m_0 is smaller in $SrBi_3$, which means that electron-electron scattering is so weak as to be ignored compared to electron-phonon scattering. Whether it is dominated by lattice symmetry or electronic behavior needs to be confirmed.

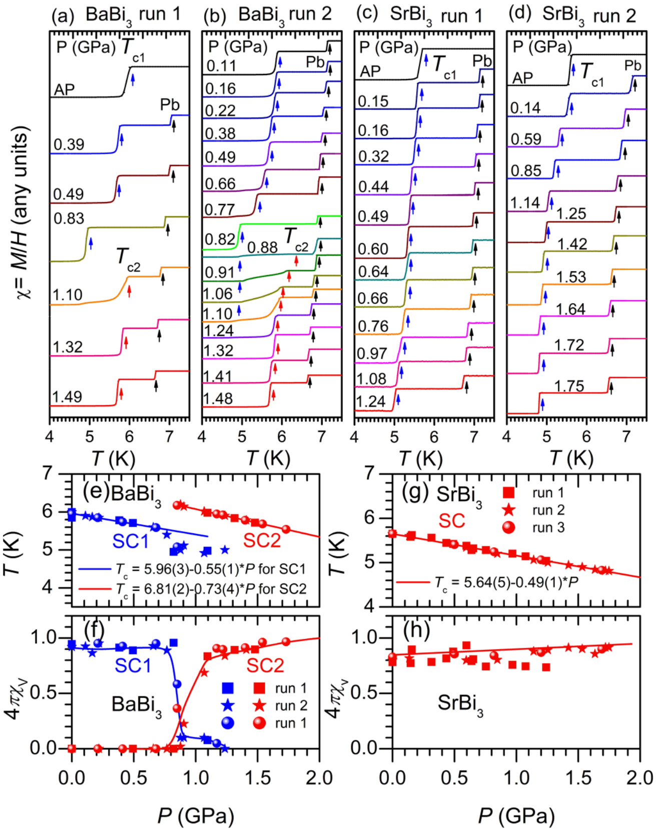

FIG. 2. $M(T)$ curves under ZFC process at 10 Oe for (a) $BaBi_3$, run 1, (b) $BaBi_3$, run 2, (c) $SrBi_3$, run 1, and (d) $SrBi_3$, run 2. T_c of (e) $BaBi_3$ and (g) $SrBi_3$. The $4\pi(M/H)$ for (f) $BaBi_3$ and (h) $SrBi_3$; the lines in (e,g) are linear fittings; the lines in (f,h) indicate the change trends.

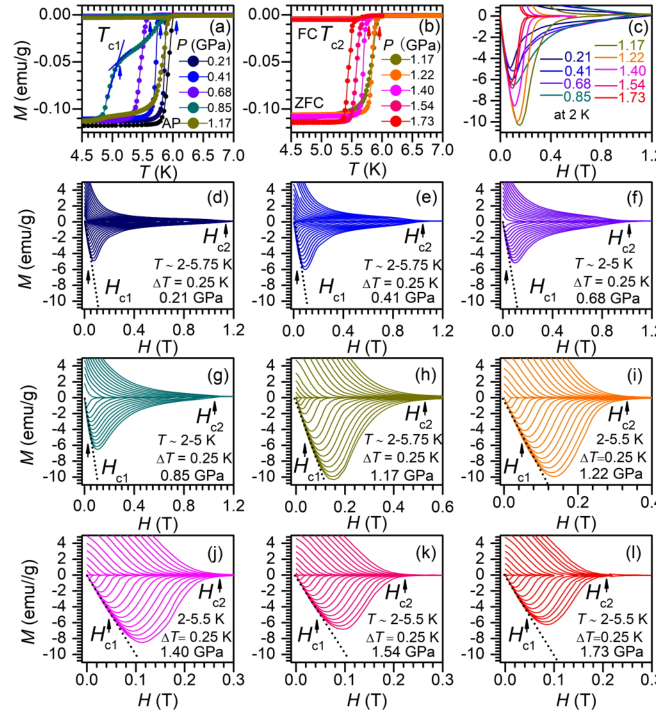

FIG. 3. (a,b) $M(T)$ curves under various pressures for $BaBi_3$; $M(H)$ curves under various temperatures/pressures: (c) 2 K; (d) 2–5.75 K at 0.21 GPa; (e) 2–5.75 K at 0.41 GPa; (f) 2–5 K at 0.68 GPa; (g) 2–5 K at 0.85 GPa; (h) 2–5.75 K at 1.17 GPa; (i) 2–5.5 K at 1.22 GPa; (j) 2–5.5 K at 1.40 GPa; (k) 2–5.5 K at 1.54 GPa; (l) 2–5.5 K at 1.73 GPa.

Superconducting parameters are obtained by analyzing the field dependence of $\rho(T)$, $M(T)$ in Fig. S1 in the Supplemental Material [22]. The upper critical field $H_{c2}(0)$ is 21.8 kOe for $BaBi_3$ and 1.9 kOe for $SrBi_3$ by using the Werthamer-Helfand-Hohenberg formula $H_{c2}(0) = -0.693\, T_c\, dH_{c2}/dT$ [23]. The lower critical field H_{c1} is determined where magnetization departs linearly (Figs. S1(c) and S1(d) [22]). Temperature-dependent $H_{c1}(T)$ data are fitted by the formula $H_{c1}(T) = H_{c1}(0)[1–(T/T_c)^2]$ and the lower critical field $H_{c1}(0)$ is 237.8 Oe for $BaBi_3$ and 488.70 Oe for $SrBi_3$ by fitting $H_{c1}(T) = H_{c1}(0)[1–(T/T_c)^2]$. Superconducting coherence length ξ is 12.30 nm for $BaBi_3$ and 42.28 nm for $SrBi_3$ by the relationship of $H_{c2}(0) = \Phi_0/2\pi\xi^2$ (where Φ_0 is the magnetic flux quantum) [24]. Then, London penetration depths λ_L and κ_{GL} are estimated by $H_{c2}/H_{c1} = 2\kappa_{GL}^2/\ln\kappa_{GL}$ and $\kappa_{GL} = \lambda_L/\xi$. $\lambda_L \sim 127.30$ nm and $\kappa_{GL} \sim 10.35$ for $BaBi_3$; $\lambda_L \sim 31.79$ nm and $\kappa_{GL} \sim 0.76$ for $SrBi_3$. We note that $\kappa_{GL} \sim 10.35$ in $BaBi_3$ is larger than that of $SrBi_3$ (~ 0.76) [1–3], which implies a possible crossover from a type-II to a type-I SC.

Temperature dependence of magnetic susceptibility under various pressures is shown in Fig. 2. Pressure dependences of T_c^M and $4\pi(M/H)$ are summarized in Figs. 2(e)–2(h). For $BaBa_3$, T_c^M decreases from 5.95 at AP to 5.08 K at 0.85 GPa, then reaches 6.2 K at $P_c \sim 0.88$ GPa, and then decreases again with increasing the pressure further. Linear fittings yield $dT_c/dP = -0.55(1)$ K/GPa for $P < P_c$ and $-0.73(4)$ K/GPa $P > P_c$. Differently, for $SrBa_3$, T_c^M decreases monotonously from 5.65 K at AP to 4.79 K at 1.75 GPa with $dT_c/dP = -0.49(1)$ K/GPa. It is noted that dT_c/dP is $\sim 2-3$ times larger in magnitude than that of Bi ($dT_c/dP = -0.18$ K/GPa) [25], which eliminates the possibilities of Bi impurity. Besides, the T_c of $BaBi_3$ was argued to increase with pressure, reaching a maximum of 6.6 K at 0.88 GPa [16]. In the case of $BaBi_3$, the present results are inconsistent with the reports. However, the reasons for this difference are not clear, either because of the quality of the samples, pressure environments, or hidden phase changes. One more interesting item is that bulk superconductivity of $BaBi_3$ vanishes at P_c with the $4\pi(M/H) \sim 5\%$ at P_c and 1 above P_c. It implies that the original superconducting state (SC1) transits into the second superconducting phase (SC2) under pressure. The $4\pi(M/H)$ of SC1 decreases from 1 to nearly zero at P_c while the $4\pi(M/H)$ of SC2 increases from zero to 1; a similar phenomenon is accompanied by pressure-induced structural transitions [26].

Pressure dependence of the superconducting parameters of $H_{c1}(0)$, $H_{c2}(0)$, $\lambda_L(0)$, $\xi(0)$, $\kappa_{GL}(0)$ are studied by measuring magnetic susceptibility. The $M(T)$ curve is shown in Figs. 3(a) and 3(b) for $BaBi_3$. The $4\pi(M/H)_{ZFC}$ and $4\pi(M/H)_{FC}$ are 100% and $\sim$5% for each P, which is the feature of type-II SCs. Accordingly, both $H_{c2}(0)$ and $H_{c1}(0)$ are calculated and summarized in Figs. 4(b) and 4(c), and Table S2 in the Supplemental Material [22]. $H_{c2}(0)$ decreases monotonously to 13.3 kOe at 0.85 GPa, then jumpily to 3.77 kOe at 1.22 GPa, and then decreases with increasing the pressure, but $H_{c1}(0)$ shows an

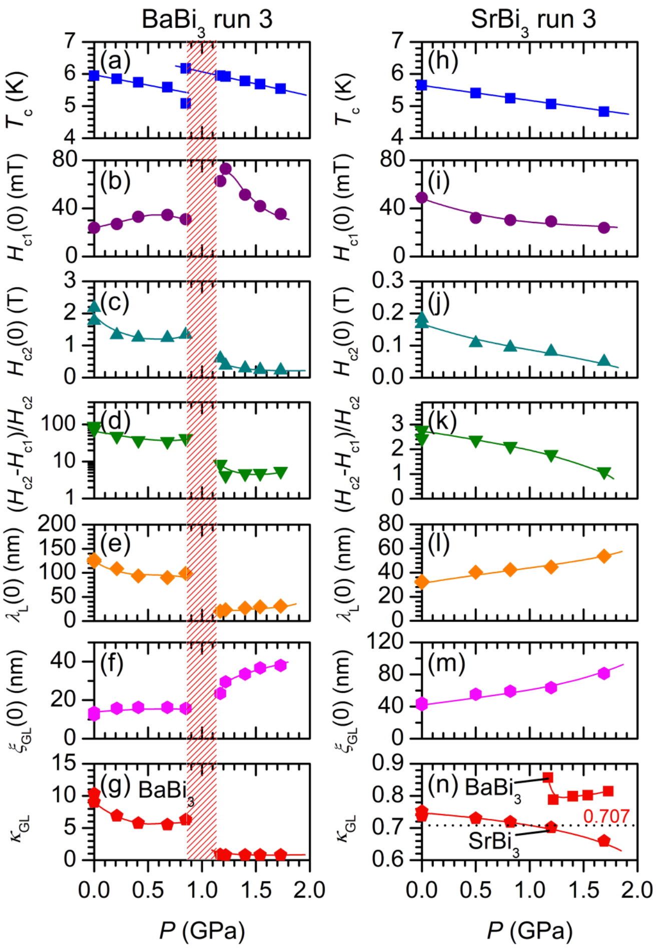

FIG. 4. Superconducting parameters with pressure: (a) T_c, (b) $H_{c1}(0)$, (c) $H_{c2}(0)$, (d) η, (e) λ_L, (f) ξ, (g) κ_{GL} for $BaBi_3$; (h) T_c, (i) $H_{c1}(0)$, (j) $H_{c2}(0)$, (k) η, (l) λ_L, (m) ξ, (n) κ_{GL} for $SrBi_3$; the dished lines indicate the change trends.

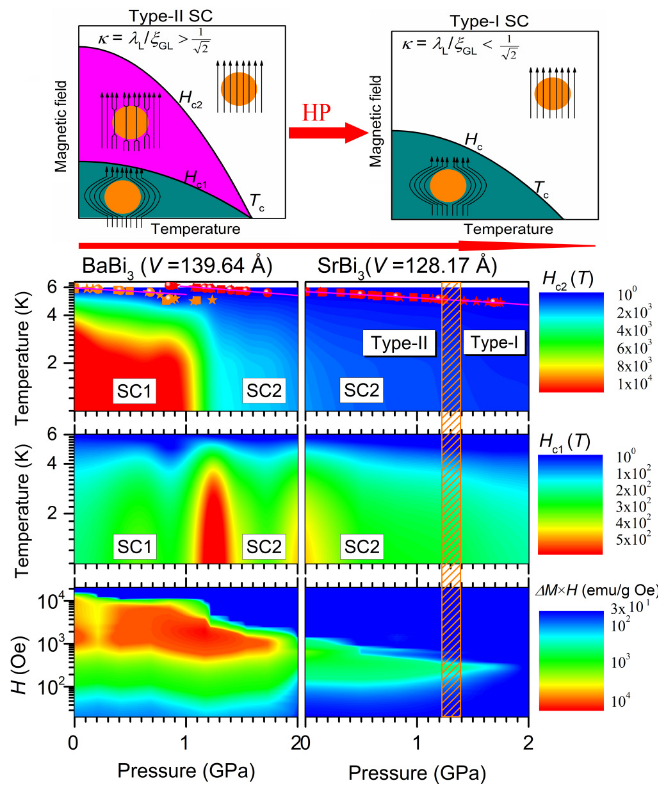

FIG. 5. Type-I SC, type-II SC, and the conversions. Pressure dependence of $H_{c1}(0)$, $H_{c2}(0)$ is plotted and the colors represent the changes of fields. Phase diagram of $P - H - \Delta M \times H$, where ΔM is the difference of hysteresis loops under the same field.

enhancement at P_c at first, and then decreases with pressure. It manifests that SC1 is more robust than SC2 [27]. Then, $\xi(0)$, $\lambda_L(0)$, and $\kappa_{GL}(0)$ are calculated in Figs. 4(e)–4(g). These parameters jump around P_c. In detail, λ_L decreases while ξ shows a monotonous increase with increasing the pressure. As a result, κ_{GL} of $BaBi_3$ decreases from 10.53 at AP to 0.86 at 1.17 GPa, and then tends to saturation. It suggests that decrease of κ_{GL} at P_c is closely related with structural transition. We note that κ_{GL} of $BaBi_3$ is larger than $\frac{1}{\sqrt{2}}$ in both SC1 and SC2, indicating that both are type-II SCs. We also focus on $M(H)$s of $BaBi_3$ as in Figs. 3(c)–3(l): it is thin and concave for SC1 and becomes plump and symmetrical for SC2, reflecting different superconducting properties. In the same way, the susceptibility of $SrBi_3$ was plotted in Fig. S2 (0.50, 0.82, 1.20, 1.69 GPa) in the Supplemental Material [22]. With increasing the pressure, the divergences of $M(T)_{ZFC}$ and $M(T)_{FC}$ decrease. As a result, the $4\pi(M/H)_{ZFC}$ remain unchanged, ~85%, while the $4\pi(M/H)_{FC}$ increases from 45% at AP to ~80% at 1.20 GPa. Figures 4(h)–4(n) show the $H_{c1}(0)$, $H_{c2}(0)\xi(0)$, $\lambda_L(0)$, and $\kappa_{GL}(0)$ as a function of pressure. It is found that $H_{c2}(0)$ and $H_{c1}(0)$ decrease until 1.69 GPa while $\xi(0)$ and $\lambda_L(0)$ increase. The κ_{GL} decreases from 0.76 at AP to 0.72 at 0.82 GPa, which approaches the typical value of $\frac{1}{\sqrt{2}}$ at 1.20 GPa. Meanwhile, the larger magnetic hysteresis decreases with increasing the pressure, and disappears above 1.20 GPa. These features are the evidence for the crossover from a type-II to a type-I SC [1,2].

Figure 5 presents type-I SC, type-II SC, and the conversion. In $BaBi_3$, from SC1 to SC2, $H_{c2}(0)$ decreases while $H_{c1}(0)$ increases around P_c, which accounts for the jump of κ_{GL}, while in $SrBi_3$, large and insensitive pressure dependence of $H_{c1}(0)$ is an inducement of the decrease in κ_{GL}. In Figs. 4(d) and 5(k), a parameter $\eta = [H_{c2}(0) - H_{c1}(0)]/H_{c2}(0)$ is used to describe the evolution of $H_{c1}(0)$ and $H_{c2}(0)$: type I ($\eta \leqslant 1$) and type II ($\eta \geqslant 1$). η decreases from 85.4 at AP to 4.18 at 1.22 GPa in $BaBi_3$, and from 2.76 at AP to $\frac{1}{\sqrt{2}}$ above 1.20 GPa in $SrBi_3$, indicating pressure-induced crossover. Type-II SC has a strong flux-pinning effect, which is not possible in a "clean" type-I SC. Thus, a type-II SC can be distinguished. In Fig. 3 and Fig. S2 in the Supplemental Material [22], ΔM is defined as the width of the hysteresis loop and is proportional to critical current density by the Bean models. In $BaBi_3$, ΔM increases at first and its value at 1.22 GPa is 2 times larger than that at AP, and then decreases with increasing the pressure. In $SrBi_3$, $\Delta M(H)$ decreases in the same shape with SC2 of $BaBi_3$ and the magnitude decreases to nearly 20 times smaller above 1.20 GPa, which suggests the pressure-induced crossover. However, an inconsistency is that the pinning effect is not completely eliminated in $SrBi_3$. One reason is the interference of impurities which makes a type-I SC behave as a type-II SC. Similar phenomena frequently appear in type-I SCs [8,9]. In addition, $\Delta M \times H$ at 2 K in Figs. S3(c) and S3(d) changes from a platform peak below P_c to a single sharp peak above P_c in $BaBi_3$ (Supplemental Material [22]). In $SrBi_3$, it decreases to nearly zero above 1.20 GPa. These characteristics confirm the crossover again.

The constructed Fermi surface along with tetragonal-cubic phase transition is critical to two district superconducting phases. In $BaBi_3$, high pressure decreases T_c but with a sudden rise at P_c. Several origins are proposed: the first scenario is that pressure broadens energy bands and results in a decrease in $N(E_F)$ [23]. It is consistent with the dominated s-wave gaps [10,11,13] and Matthias rules [15]. The second factor is SOC, which is conducive to superconducting pairs and causes an increase of the electron-phonon coupling and $N(E_F)$ [13]. T_c decreases if SOC is suppressed by pressure. Thirdly, the increase of T_c at P_c is unusual in $BaBi_3$. As above, the features of SC2 in $BaBi_3$ are similar to those of $SrBi_3$, giving us a convincing reason to believe that structural transition causes the increase of T_c comparable to the Na doping [15]. Similar behaviors have been reported in CaC_6 and Bi [26,28,29]. One more interesting item is the crossover from type-II to type-I SC in $SrBi_3$. It has been argued that a type-I SC can be converted into a type-II SC by introducing impurities [5,6]. Because disorders shorten electron mean free path and lead to the increases of κ_{GL} in the "dirty"-limit SCs. Thus, this crossover is inclined to be an electronic transition since high pressure is a clean method [2,3]. Several mechanisms are possible: The first is that pressure reshapes bands and enhances carrier concentration. One result is to shorten the electron mean free path, which goes against the crossover in the dirty limit. However, κ_{GL} is not related with the electron mean free path in the "clean" limit. If this assumption is true, κ_{GL} is inclined to be related with $H_{c1}(0)$ and $\lambda_L(0)$, which is consistent with the above discussions. The second is the weakness of SOC and the electron-phonon coupling, which weakens electron correlations [11,13]. The third scenario is the varieties of vortex interactions along with lattice contractions, which has been predicted [7]. To clarify this, more theoretical/experimental studies are required.

We thank S. Nagasaki and Dr. Gouchi for the technical assistance. This work is supported by National Key Research and Development Program under Contracts No. 2016YFA0300404, No. 2018YFA0305700, and No. 2018FA0305800; the National Nature Science Foundation of China under Contracts No. 11674326 and No. 11874357; and the Joint Funds of the National Natural Science Foundation of China and the Chinese Academy of Sciences' Large-Scale Scientific Facility (U1832141). We also acknowledge the Strategic Priority Research Program and the Key Research Program of Frontier Sciences of CAS (XDB07020100 and QYZDB-SSW-SLH013), the IOP Hundred-Talent Program (Y7K5031 × 61), and the Youth Promotion Association, CAS (2018010).

[1] A. A. Abrikosov, Sov. Phys. JETP **5**, 1174 (1957); B. B. Goodman, Prog. Phys. **29**, 445 (1966).
[2] R. Khasanov, P. S. Häfliger, N. Shitsevalova, A. Dukhnenko, R. Brütsch, and H. Keller, Phys. Rev. Lett. **97**, 157002 (2006); S. Gabáni, Mat. Orendáč, J. Kušnír, E. Gažo, G. Pristáš, T. Mori, and K. Flachbart, J. Low Temp. Phys. **187**, 559 (2017).
[3] K. E. Gray, J. Zasadzinski, R. Vaglio, and D. Hinks, Phys. Rev. B **27**, 4161 (1983).
[4] H. W. Weber, J. F. Sporna, and E. Seidl, Phys. Rev. Lett. **41**, 1502 (1978).
[5] H. Kiessig, U. Essmann, H. Teichler, and W. Wiethaup, Phys. Lett. A **51**, 333 (1975).
[6] J. Auer and H. Ullmaier, Phys. Rev. B **7**, 136 (1973).
[7] J. Hove, S. Mo, and A. Sudbo, Phys. Rev. B **66**, 064524 (2002).
[8] Z. Wang, Y. Sun, X. Q. Chen, C. Franchini, G. Xu, H. M. Weng, X. Dai, and Z. Fang, Phys. Rev. B **85**, 195320 (2012).
[9] X. Zhu, H. Lei, C. Petrovic, and Y. Zhang, Phys. Rev. B **86**, 024527 (2012).
[10] B. T. Matthias and K. Corenzwit, Phys. Rev. **107**, 1558 (1957).
[11] N. Haldolaarachchige, S. K. Kushwaha, Q. Gibson, and R. J. Cava, Supercond. Sci. Technol. **27**, 105001 (2014).
[12] B. T. Matthias and J. K. Hulm, Phys. Rev. **87**, 799 (1952).
[13] D. F. Shao, X. Luo, W. J. Luo, L. Hu, X. D. Zhu, W. H. Song, X. B. Zhu, and Y. P. Sun, Sci. Rep. **6**, 21484 (2016).
[14] M. J. Winiarski, B. Wiendlocha, S. Golab, S. K. Kushwaha, P. Wisniewski, D. Kaczorowski, J. D. Thompson, R. J. Cava, and T. Klimczuk, Phys. Chem. Chem. Phys. **18**, 21737 (2016).
[15] A. Iyo, Y. Yanagi, T. Kinjo, T. Nishio, I. Hase, T. Yanagisawa, S. Ishida, H. Kito, N. Takeshita, K. Oka, Y. Yoshida, and H. Eisaki, Sci. Rep. **5**, 10089 (2015).
[16] R. Jha, M. A. Avila, and R. A. Ribeiro, Supercond. Sci. Technol. **30**, 025015 (2017).
[17] N. Mori, H. Takahashi, and N. Takeshita, High Pressure Res. **24**, 225 (2004).
[18] W. L. McMillan, Phys. Rev. **167**, 331 (1968).
[19] K. Miyake, T. Matsuura, and C. M. Varma, Solid State Commun. **71**, 1149 (1989).
[20] S. Y. Li, L. Taillefer, D. G. Hawthorn, M. A. Tanatar, J. Paglione, M. Sutherland, R. W. Hill, C. H. Wang, and X. H. Chen, Phys. Rev. Lett. **93**, 056401 (2004).
[21] P. Tong, Y. P. Sun, X. B. Zhu, and W. H. Song, Phys. Rev. B **74**, 224416 (2006).
[22] See Supplemental Material at http://link.aps.org/supplemental/10.1103/PhysRevB.98.220506 for the summary of electrical transport and magnetic susceptibility superconducting parameters at ambient pressure and high pressure.
[23] N. R. Werthamer, E. Helfand, and P. C. Hohenberg, Phys. Rev. **147**, 295 (1966).
[24] J. Bardeen, L. N. Cooper, and J. R. Schrieffer, Phys. Rev. **108**, 1175 (1957).
[25] C. Buzea and K. Robbie, Supercond. Sci. Technol. **18**, R1 (2005).
[26] K. Kudo, M. Takasuga, Y. Okamoto, Z. Hiroi, and M. Nohara, Phys. Rev. Lett. **109**, 097002 (2012).
[27] I. J. Lee, M. J. Naughton, G. M. Danner, and P. M. Chaikin, Phys. Rev. Lett. **78**, 3555 (1997).
[28] A. Gauzzi, S. Takashima, N. Takeshita, C. Terakura, H. Takagi, N. Emery, C. Herold, P. Lagrange, and G. Loupias, Phys. Rev. Lett. **98**, 067002 (2007).
[29] A. Yoneda and S. Endo, J. Appl. Phys. **51**, 3216 (1980).